Available online at www.sciencedirect.com
SCIENCE DIRECT®
Pergamon
International Journal of Machine Tools & Manufacture 43 (2003) 605–615
INTERNATIONAL JOURNAL OF MACHINE TOOLS & MANUFACTURE
DESIGN, RESEARCH AND APPLICATION

Thermal modeling of friction stir welding in a moving coordinate system and its validation

M. Song, R. Kovacevic *

Research Center for Advanced Manufacturing, Department of Mechanical Engineering, Southern Methodist University, 1500 International PKW, Suit 100, Richardson, TX, 75081, USA

Received 21 October 2002; accepted 20 December 2002

Abstract

A three-dimensional heat transfer model for friction stir welding (FSW) is presented in this paper; a moving coordinate is introduced to reduce the difficulty of modeling the moving tool. Heat input from the tool shoulder and the tool pin are considered in the model. The finite difference method was applied in solving the control equations. A non-uniform grid mesh is generated for the calculation. FSW experiments have been done to validate the calculated results. The calculated results are in good agreement with the experimental results. The calculation result also shows that preheat to the workpiece is beneficial to FSW.

Keywords: Friction stir welding; Heat transfer; Modeling; Aluminum alloy; Welding

1. Introduction

Friction stir welding (FSW) is a new solid-state joining technology invented at the welding institute (TWI) in 1991 [1]. It has been proven to be a very successful joining technology for aluminum alloys. Friction stir welding of nickel alloys and steel is also promising [2,3]. Compared to the conventional welding processes, FSW can produce superior mechanical properties in the weld zone. This new technique is being successfully applied to the aerospace, automobile, and shipbuilding industries [4], and is attracting more and more research interest.

The heat transfer process is one of the most important aspects in the FSW study. A good understanding of the heat transfer process in the workpiece can be helpful in predicting the thermal cycles in the welding workpiece, and the hardness in the weld zone, subsequently, can be helpful in evaluating the weld quality. A known temperature distribution is also important for calculating the temperature-dependent viscosity when modeling material flow.

Significant progress has recently been made on heat transfer modeling for FSW [5–19]. The thermal couple measured temperature history of the workpiece during FSW has also been attained [20–23].

Chao and Qi [5] published a three-dimensional heat transfer model in 1998, in their paper, a constant heat flux input from the tool shoulder/workpiece interface was assumed, a trial-and-error procedure was used to adjust the heat input until the all the calculated temperatures matches with the measured ones. Frigaard, Grong, and Midling [6,7] developed a process model for FSW, the heat input from the tool shoulder is assumed to be the frictional heat, and the coefficient of friction or the calculated temperature during the welding is adjusted to keep the calculated temperature from exceeding the material melting point.

The Rosenthal equation for modeling heat-transfer for thin plates has also been applied in modeling the heat-transfer in FSW [8,9]. Zahedul, Khandkar, and Khan modeled the heat transfer for overlap friction stir welding with the finite element method; a moving heat source is used [10]. Bendzsak, North, and Smith et al. applied the CFD method in modeling the heat and material flow process for FSW, where the material is assumed to be a kind of non-Newtonian fluid in their modeling [11,12].

In the above-mentioned models, the heat input from the tool shoulder is the only heat input, the heat gener-

* Corresponding author. Fax: +1-214-768-0812.
E-mail address: kovacevi@engr.smu.edu (R. Kovacevic).

0890-6955/03/$ - see front matter © 2003 Elsevier Science Ltd. All rights reserved.
doi:10.1016/S0890-6955(03)00022-1

Nomenclature

c	heat capacity, J/K_gK
F_f	surface friction force, N
F_n	normal force, N
F_p	translation force, N
h	thickness of the workpiece, m
h_c	coefficient of heat convection, W/m^2K
H	enthalpy, J/Kg J/Kg
k_x, k_y, k_z	thermal conductivity, W/mK
n	normal vector of boundary Γ
q	heat flux, W/m^2
r_p	radius of the pin, m
r_{sh}	radius of the shoulder, m
S	heat source term, W/m^3
t	time, sec
T	temperature, K
v_i	slip velocity, m/sec
v_w	welding speed, m/sec
x,y,z	space coordinate, m
$\bar{Y}$	average yield stress, MPa
λ	helix angle of the pin thread
μ	coefficient of friction

ated at the tool pin / workpiece interface has not been included.

Heat generated by the pin was estimated to be only 2% of the total heat generation during the FSW [9]; however, this ration was estimated to be up to 20% by some researchers [13], In order to model the heat transfer process accurately, it is necessary to include the heat generated by the tool pin in the modeling.

The heat transfer process during the tool penetration period cannot be modeled if the heat input from the pin is not included. Moreover, the initial field is very important in a transient heat transfer model, especially for modeling the preheat effects of laser-assisted preheated FSW [14]. For this purpose, the heat transfer during the tool penetration period cannot be neglected.

During the FSW process the tool penetrates into the workpiece, then moves along the joint line at a constant speed (see Fig. 1). The material in front of the rotating tool pin is plastically deformed and stirred back to the trail edge of the tool pin in the welding. This continuous "stir" process makes it difficult to model the heat input from the pin. First, the material plastic flow process is very complicated, making it almost impossible to determine the temperature distribution of the relocated material that is stirred from the front edge to the aft edge of the tool pin. Secondly, the tool pin is non-consumable in the welding, and modeling a moving tool pin in the workpiece is also not easy. The heat input from the tool pin is simplified as a moving heat source [15]; however, this assumption is not helpful in modeling the coupled heat transfer for both the tool and the workpiece.

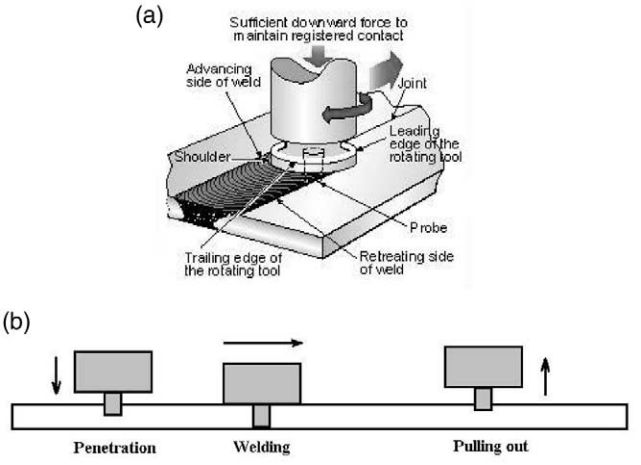

Fig. 1. Schematic diagram of FSW [2].

In this paper, a moving coordinate has been introduced to model the transient three-dimensional heat transfer process for FSW. The coordinate is chosen stationary with the moving tool. Therefore, the difficulty of modeling the complicated stir process can be greatly reduced, thus making this model more accurate.

2. Mathematical model

In this paper, the FSW process is divided into the following three periods: the penetration period, the weld period, and the tool pulling out period [15], as shown in Fig. 1. The following assumptions are introduced in the model:

1. The heat generated at the tool shoulder/workpiece interface is frictional heat;
2. The tool pin is a cylinder; the thread of the pin can be neglected;
3. No heat flows into the workpiece if the local temperature reaches the material melting temperature.

2.1. Control equation in a moving coordinate

During the main friction stir welding process, or the weld period, the tool is moving at a constant speed along the joint line. For such a problem, it is convenient to use a moving coordinate system that moves with the tool, instead of using a stationary system. By applying a moving coordinate, it is not necessary to model the complicated stir process near the pin, thus it makes the model easier.

The heat transfer control equation for the workpiece in a moving coordinate system with a positive x-direction moving tool can be written as:

$$\frac{\partial(\rho\, c\, T)}{\partial\, t} = \frac{\partial}{\partial x}(k_x\frac{\partial T}{\partial\, x}) + \frac{\partial}{\partial y}(k_y\frac{\partial T}{\partial\, \mathrm{y}}) + \frac{\partial}{\partial z}(k_z\frac{\partial T}{\partial\, \mathrm{z}}) + v_w\frac{\partial(\rho c T)}{\partial x} \tag{1}$$

Where T is the temperature, c is the heat capacity, ρ is the density, k is the heat conductivity, and v is the tool moving speed.

2.2. Heat generation

In the presented model, the heat at the tool shoulder/workpiece interface and the heat at the tool pin/workpiece interface are both considered.

2.2.1. Heat input from the tool shoulder

The heat generated at the tool shoulder/workpiece interface is assumed the frictional work in this model. The local heat generation can be calculated by the following expression [15]:

$$q_{f\,i} = 2\pi\mu F_n R_i n \tag{2}$$

Where R_i is the distance from the calculated point to the axis of the rotating tool, n is the rotational speed of the tool.

The coefficient of the friction is believed to vary during the FSW process; the detail of the variation is still not clear so far. An effective coefficient of friction is assumed in this model.

2.2.2. Heat input from the tool pin

The heat generated by the tool pin consists of the following three parts: (1) heat generated by shearing of the material; (2) heat generated by the friction on the threaded surface of the pin; and (3) heat generated by friction on the vertical surface of the pin. Colegrove gave an expression on calculating the heat generated from the pin [13].

$$Q_{pin} = 2\pi r_p h k\bar{Y}\frac{V_m}{\sqrt{3}} + \frac{2\mu\, k\bar{Y}\pi r_p h V_{rp}}{\sqrt{3(1+\mu^2)}} + \frac{4F_p\mu V_m\cos\theta}{\pi} \tag{3}$$

Where $\theta = 90^\circ-\lambda-\tan^{-1}(\mu)$, $V_m = \dfrac{\sin\lambda}{\sin(180^\circ-\theta-\lambda)}v_p$, $V_{rp} = \dfrac{\sin\theta}{\sin(180^\circ-\theta-\lambda)}v_p$, and $v_p = r_p\omega$. r_p is the radius of the tool pin, h is the thickness of the workpiece, $\bar{Y}$ is the average shear stress of the material, F_p is the translation force during the welding, and λ is the helix angle of the thread, and μ is the friction coefficient.

Because the tool pin is assumed to be a cylinder with no thread, only the first item in Eq. (3) is calculated as the heat input from the tool pin.

2.3. Boundary conditions and initial condition

2.3.1. Tool shoulder/workpiece interface

The heat flux boundary condition for the workpiece at the tool shoulder/workpiece interface is

$$k\frac{\partial T}{\partial n}\bigg|_\Gamma = q_S \tag{4}$$

2.3.2. Tool pin/workpiece interface

The heat flux boundary condition at the tool pin / workpiece interface is similar to the tool shoulder / workpiece interface, and can be written as

$$k\frac{\partial T}{\partial n}\bigg|_\Gamma = q_P \tag{5}$$

q_s and q_p can be calculated by Eqs. (2) and (3).

2.3.3. The convection boundary conditions

The convection boundary condition for all the workpiece surfaces exposed to the air can be expressed as

$$k\frac{\partial T}{\partial n}\bigg|_\Gamma = h(T-T_0) \tag{6}$$

Where n is the normal direction vector of boundary Γ,

and h is the convection coefficient. The surface of the workpiece in contact with the backup plate is simplified to the convection condition with an effective convection coefficient in this model.

Fig. 2 illustrates all the boundary conditions for the calculations.

2.3.4. Symmetric boundary conditions

In the friction stir welding process, the two plates are welded along the joint line in aft of the tool, but not welded yet in front of the tool. In this paper, the boundary condition at the joint line is a symmetric boundary condition in aft of the tool pin:

$$T_{j=1} = T_{j=2} \tag{7}$$

and is simplified to the convection boundary condition in front of the tool:

$$k\frac{\partial T}{\partial n}\bigg|_{\Gamma} = h(T-T_0) \tag{8}$$

Actually the joint surface of the two plates is a faying surface before the tool passes by.

2.3.5. Tool penetration and extraction

During the processes of the tool penetration and pulling out, the height of the tool pin penetrating into the workpiece, dz, representing the height of the heat flux applied area, varies from 0 to h_p. The height can be calculated by the tool penetration and extraction speeds, respectively. The height is:

$$dz = v_p dt \tag{9}$$

during the penetration period, and:

$$dz = h_p - v_{ex} dt \tag{10}$$

during the pulling out period. Where v_p and v_{ex} are the tool pin penetration and extraction speeds, respectively.

Because a moving coordinate is introduced, the heat source is static in the calculation, except during the pin penetration and pulling out periods. Because the heat transfer during the tool pulling out period is not important in modeling the heat transfer process of FSW, thus it has not been discussed in this paper.

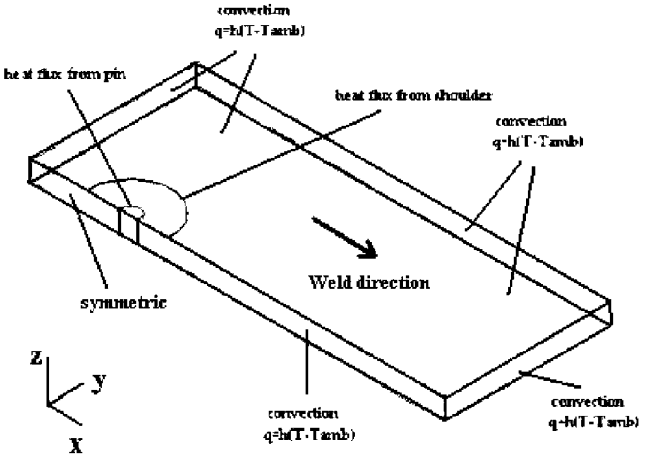

Fig. 2. Boundary conditions in the presented heat transfer model.

2.3.6. Initial condition

The initial condition for the calculation is:

$$T(x,y,z,0) = T_i \tag{11}$$

3. Numerical solution

The heat transfer control equations are solved numerically with a finite difference method. Because the two plates to be welded are symmetric, only one plate is modeled.

FSW is believed to be a solid-state weld. In order to keep the calculated temperature from exceeding the material melting temperature, the heat flux is adjusted to zero if the calculated temperature reaches the material melting temperature. Because the temperature gradient at the surface will be very small if the temperature reaches the melting temperature, therefore, this is a good assumption.

3.1. Non-uniform grid

Because the dimension of the tool pin is relatively small compared with the dimension of the workpiece. In order to get an accurate result, it is better to put more grid nodes near the tool pin. A non-uniform grid mesh has been generated in this paper to ensure enough grid nodes are put near the tool pin, as shown in Fig. 2. The following expressions are introduced in generating the non-uniform grid:

$$dx_i = \varepsilon_1 dx_{i-1} \tag{12}$$

$$dy_j = \varepsilon_2 dy_{j-1} \tag{13}$$

$$dz_k = \varepsilon_3 dz_{k-1} \tag{14}$$

3.2. Numerical scheme

The heat transfer control equation was discretized by an explicit central difference scheme. The second-order derivative of the temperature in x-direction in the non-uniform grid for all inner points is:

$$\frac{\partial^2 T_{i,j,k}}{\partial^2 x} = 2\left\{\frac{T_{i+1,j,k}dx(i-1) + T_{i-1,j,k}dx(i) - T_{i,j,k}[dx(i) + dx(i-1)]}{[dx(i) + dx(i-1)][dx(i)][dx(i-1)]}\right\} \tag{15}$$

The first-order derivative of the temperature in the x-direction in the non-uniform grid for all inner points is:

$$\frac{\partial T_{i,j,k}}{\partial x} = \frac{T_{i+1,j,k} - T_{i,j,k}}{dx(i-1)} \tag{16}$$

The second-order derivative of the temperature in the y-direction and the z-direction can be expressed in the similar way.

Denoting $\frac{\partial^2 T_{i,j,k}}{\partial^2 x}$ as $TEM^2(x)$, and $\frac{\partial T_{i,j,k}}{\partial x}$ as $TEM\ (x)$, the time marching procedures for all inner points are:

$$T_{i,j,k}^{(n+1)} = T_{i,j,k}^{(n)} + \frac{\Delta t}{\rho c}[k_x TEM^2(x) + k_y TEM^2(y) + k_x TEM^2(z)] + vTEM(x)\Delta t \tag{17}$$

Where $T_{i,j,k}^{(n)}$ and $T_{i,j,k}^{(n+1)}$ are the temperatures at point (i,j,k) at time n and $n+1$, respectively, $dx(i)$ is the non-uniform grid space at node (i,j,k), $TEM(x)$ is the first order derivative to x, $TEM^2(x)$ is the second order derivative to x, Δt is time marching step in the calculation.

In the calculation, if the calculated temperature reaches the material melting temperature, the heat input from the tool is adjusted to zero:

$$q = 0 \qquad (T \geq T_{melt}) \tag{18}$$

3.3. Boundary condition

There are three kinds of boundary conditions in the model, the heat flux boundary condition, the convection boundary condition, and the symmetric boundary condition.

The discretization of the heat-flux boundary condition at the tool shoulder/workpiece contact surface is:

$$T_{i,nj,k}^{(n)} = T_{i,nj-1,k}^{(n)} + q_f \Delta x / k \tag{19}$$

The discretization of the convection boundary condition in other area on the workpiece upper surface is:

$$T_{i,nj,k}^{(n)} = \frac{k_y T_{i,nj-1,k}^{(n)} + h\Delta y T_0}{k_y + h\Delta y} \tag{20}$$

Similar boundary discretizations are applied to all other boundaries.

The heat-flux boundary condition is applied only to the points within the tool shoulder covered workpiece top surface (j = nj). The heat-flux boundary condition is restricted to a circular area, where all points within this circular area from the tool axis is smaller than the tool shoulder radius r_{sh} (see Fig. 3):

$$dist_1 = \sqrt{(x_{i,j,nk} - x_{i0,j0,nk})^2 + (y_{i,j,nk} - y_{i0,j0,nk})^2} \leq r_{sh} \tag{21}$$

(i = 2,3,…ni - 1, j = 2,3,…nj - 1)

A similar rule is applied in determining the heat-flux boundary of the tool pin, the approximation of the tool boundary is shown in Fig. 3.

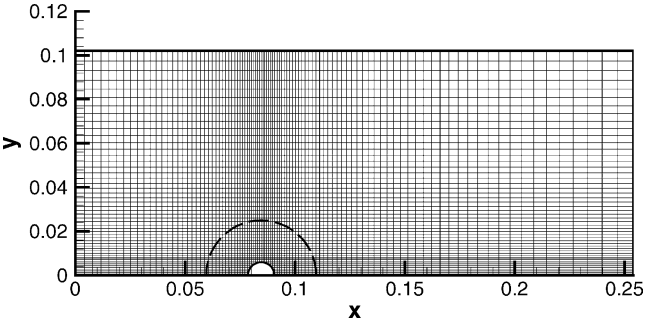

Fig. 3. The non-uniform grid mesh for the calculations, top view.

The symmetric boundary condition at the joint line can be simplified as:

$$T_{i,1,k} = T_{i,2,k} \tag{22}$$

During the tool penetration and pulling out periods, the heights of the heat-flux boundary representing the tool pin moves at the tool penetration and the pulling out speed respectively.

$$dz = v_p dt \tag{23}$$

$$dz = v_{po} dt \tag{24}$$

Where v_p and v_{po} are the tool pin-penetration speed and tool pulling-out speed, respectively.

3.4. Material properties and welding conditions

The heat conduction coefficients k_x, k_y, and k_z are assumed constant and equal during the welding. The material properties of the Al 6061/T6, and the welding conditions used in the calculations are listed in Table 1, Table 2.

4. Results and discussion

The workpiece to be friction stir welded is a pair of Al 6061-T6 plates, with a dimension of 254 x 102 x 12.7 mm, respectively. The tool is made of H-13 tool steel, the tool pin is 6 mm in radius, and 12 mm in height; the tool shoulder is 50 mm in radius, and 50 mm in height.

A 80 x 50 x 15 grid is used in the calculation. The time marching step is 0.01 s. The calculated temperature history is compared with the thermal couple measured data. The calculated maximum temperature distribution of the weld is also compared with the experimental microstructure morphology. To better describe the calculated results, the calculated data has been mirrored to the joint line in corresponding figures. FSW with and without preheat has also been calculated and discussed in this paper.

Table 1
Input data for the calculation

Density	Heat conductivity	Coeffficient of friction	Rotation speed	Weld speed	Applied force
2700 kg/m^3	167 W/m K	0.4	637 rpm	1.59 mm/s	25 KN

Table 2
Mechanical properties of 6061-T6 Aluminum

Temperature (K)	311	339	366	394	422	450	477	533	589	644
Yield Stress (MPa)	241	238	232	223	189	138	92	34	19	12

4.1. Calculated temperature contour

The temperature contour during the penetration period and the weld period was calculated and discussed.

4.1.1. Penetration period

During this period, the rotating tool pin penetrates into the workpiece, until the tool shoulder contacts the workpiece. The penetration speed is chosen to be 5 mm/s in the calculation, and the corresponding penetration time is approximately 2.54 s. The weld speed v_w is 0 in this period.

Fig. 4 shows the calculated temperature contours (front view) at different times during the penetration period. The figures graphically illustrate the temperature history of the workpiece during the pin penetration. The details of the temperature distribution near the pin in this period are shown in Fig. 5.

4.1.2. Weld period

During this period, the tool traverses along the joint line at a constant weld speed. The calculated front view section temperature contours, where the pin just passed by, at 12.0, 15.0, 22.0, and 30.0 s in the weld period as shown in Fig. 6. Fig. 7 shows the calculated temperature contours from the top view. The heat-transfer process in the weld period can be clearly found from Figs. 6 and 7. From Fig. 6, it can be found that the calculated temperature contour at 22.0 s is similar to that at time 30.0 s, which implies that a steady heat transfer could be reached at the main FSW process. Fig. 8 shows the detailed temperature distribution near the tool pin.

Fig. 9 is the 3-D view of the calculated temperature contour at time 30.0 s in the weld period.

4.2. Experimental validation

In order to verify the presented model, FSW experiments have also been done. The calculated results are compared with the experimental measured ones. Fig. 10 is the diagram of the FSW experiment setup. The temperature histories of the workpiece have been measured by Type-K NiAl/NiCr thermocouples. An infrared camera is also used to take the surface temperature of the workpiece in front of the tool, as shown in Fig. 10.

4.2.1. Comparison to the microstructure morphology

The microstructure morphology in the welding zone is believed to be related to the local thermal cycles. Typically, the FSW microstructural morphology consists of the following zones: the nugget zone, the thermal-mechanical-affected zone (TMAZ), the heat-affected zone (HAZ), and the base-material zone. The shapes and gray levels of the microstructure morphology in the cross-section area of the weld are related to the local peak temperature experienced in each region.

Fig. 11 shows the calculated temperature contours of the peak temperatures of the welding cross section, compared to the experimentally-obtained microstructure morphology. The tool rotational speed is 637 rpm; the

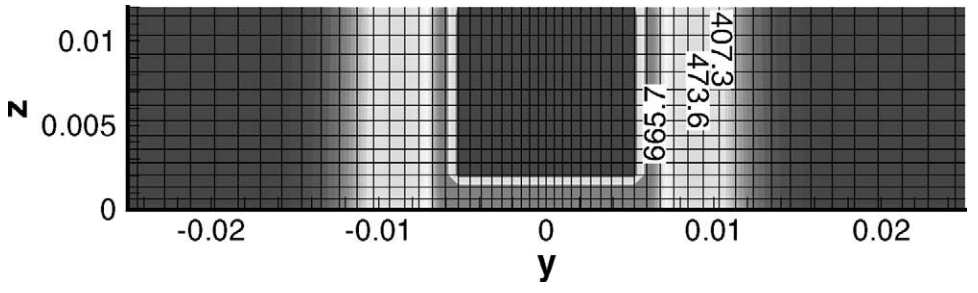

Fig. 4. Calculated isothermal during penetration period, front view.

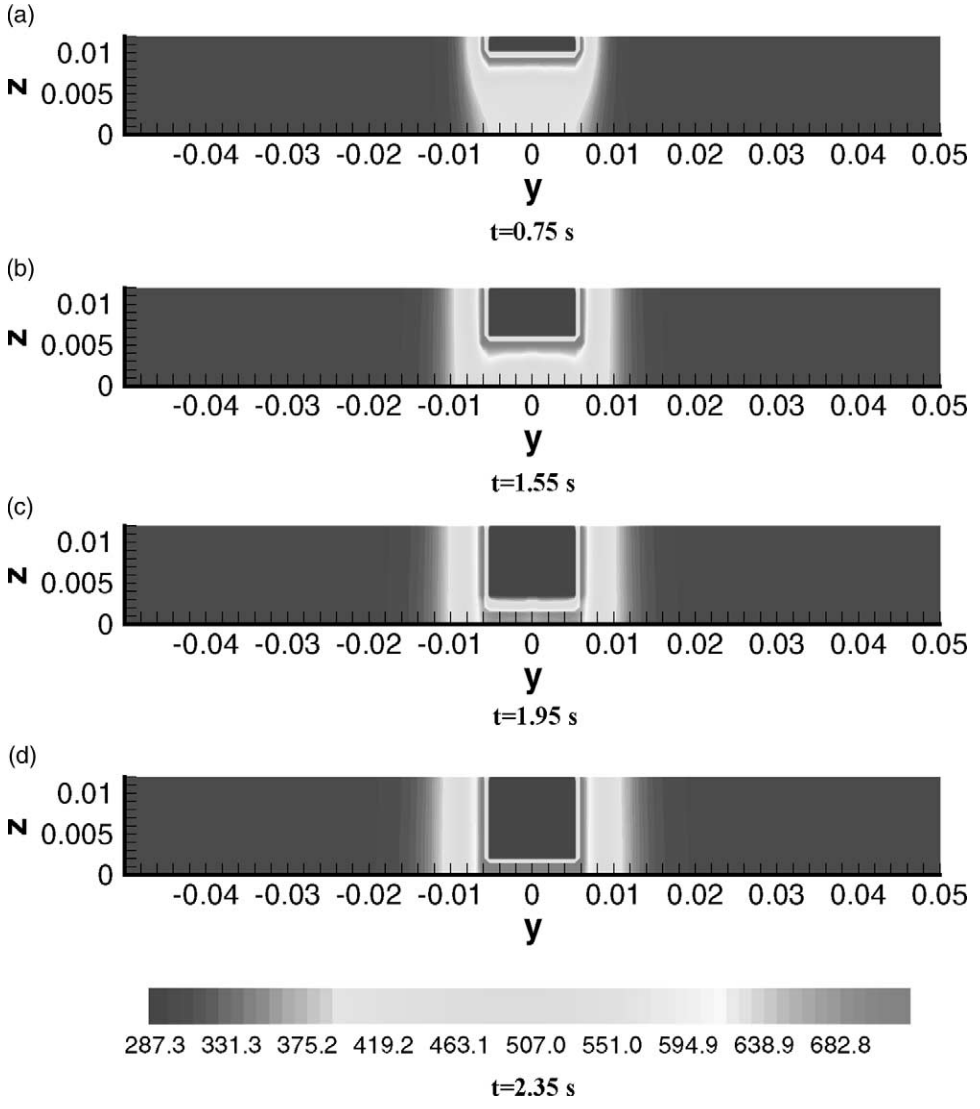

Fig. 5. Detailed results at $t = 2.35$ s in the penetration period, front view.

welding speed is 1.59 mm/s. The calculated temperature field corresponds to the main welding period, at $t = 30$ s. It can be seen that the calculated peak temperature contours can accurately simulate the temperature history of the welding zone.

The value of the calculated peak temperature in the nugget is about 820 K, the calculated peak temperature of the TMAZ is in the range of 751–612 K, and the calculated peak temperature in the HAZ is in the range of 612–439 K. The calculated temperatures in each weld zone coincide with the experimental measured results by Sato, Kokawa, Enomoto, and Jogan, for Al 6063[23], which is similar to Al 6061 in chemical composition and physical properties.

4.2.2. Comparison to the infrared camera image

Fig. 12 shows the comparison between the calculated isothermals at the top surface of workpiece, and the gray-level image of the surface temperature distribution taken by the infrared camera.

It should be noted that in Fig. 12(b), the calculated result in Zone A cannot be recorded by the infrared camera, because this area is hidden by the tool, and is infrared impenetrable. Only the measured temperature image in front of the tool shoulder can be used to compare with the calculated results (Zone B). The measured gray-level temperature image is very similar to the calculated temperature contour at the corresponding region.

From Fig. 12, it can be seen that although the detailed information beneath the tool shoulder cannot be detected by experiments, however, detailed information can be provided by the modeling results. This information is one of the advantages of numerical modeling.

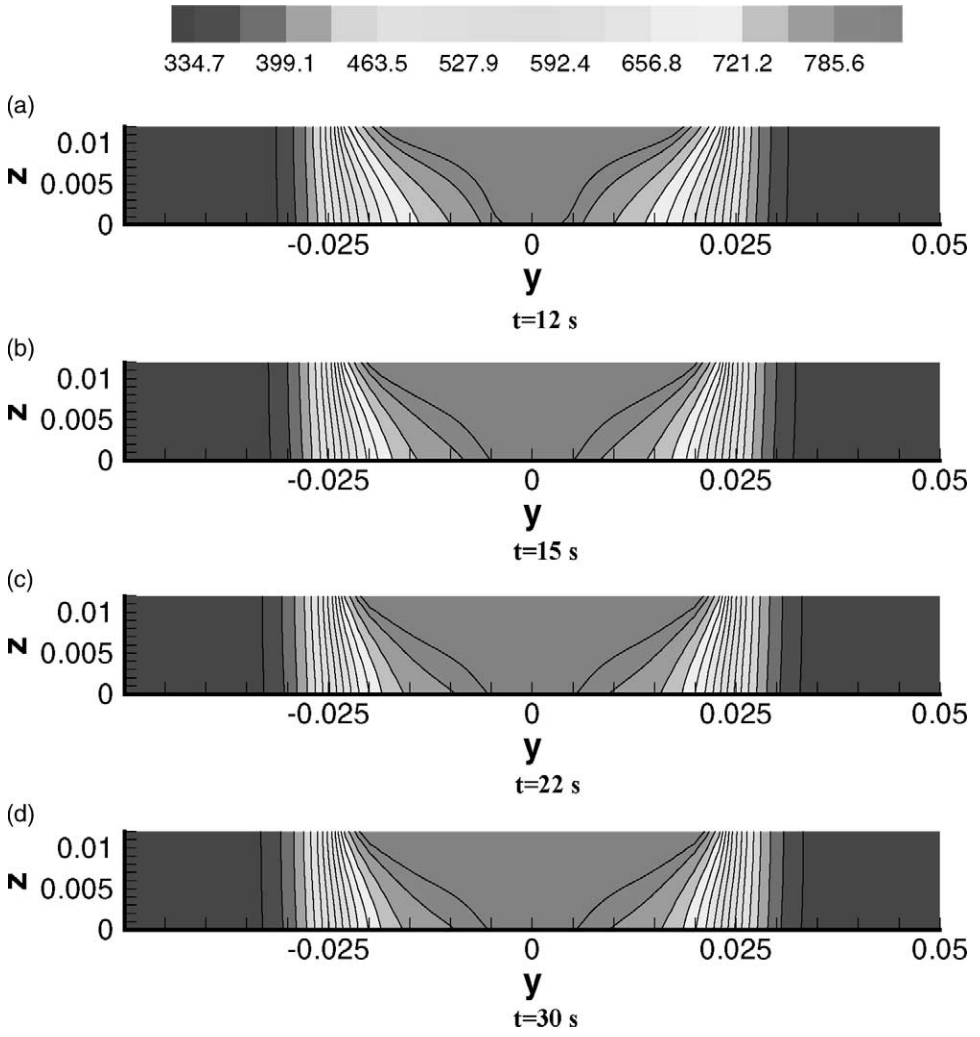

Fig. 6. Calculated isothermals during welding period, front view.

4.2.3. Comparison to the thermal couple measured results

Fig. 13 shows the comparison of the thermocouple measured and calculated temperature histories at a measuring point (114.4, 89.6, 2.5 mm). The calculated result is in good agreement with the measured one, but a little higher. Fig. 13 indicates that the presented heat-transfer model can be applied successfully in predicting the thermal cycles of the workpiece during FSW. By coupling this model to the corresponding microstructure models, the calculated temperature history can also be used in predicting the hardness in the weld zone [6,7,24].

4.3. Further discussion

One of the important research aspects of FSW is how to improve the weldability of the material, especially for alloys with high melting points, such as nickel alloys, and titanium alloys, and how to protect the tool in FSW. For most alloys, the yield stress strongly depends on the temperature. Table 2 shows the yield stress of Al 6061-T6 at different temperatures [25]. It can be seen that the yield stress of Al 6061-T6 greatly decreased at a higher temperature, which made the material easy to be friction stir welded at a higher temperature.

The following approaches can be used to get a higher initial temperature in the workpiece during FSW: (1) using an insulated backing plate to reduce the heat loss, and therefore get a higher initial temperature [7,10], and (2) applying the laser to assist preheating the workpiece during FSW [14].

In this paper, the effects of preheat by the heat from the tool shoulder is discussed. After the tool shoulder contacts the workpiece top surface, the workpiece can be preheated by making the tool rotate and stand steady for a period of time before moving. The time the static stand lasts is denoted as the preheat time. Fig. 14 shows the temperature distribution in the workpiece at different preheat times, 0, 1.0, and 2.0 s (side view). It can easily be found that the initial temperature of the workpiece in front of the tool pin can be greatly increased at a longer preheat time, and this temperature increase can reduce

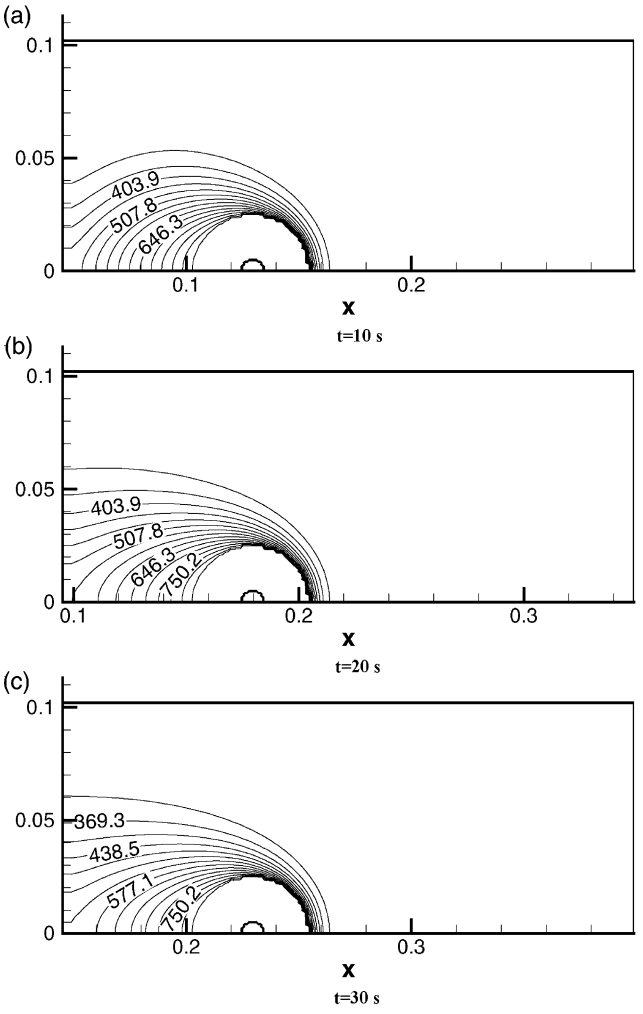

Fig. 7. Calculated isothermals during the welding period, top view.

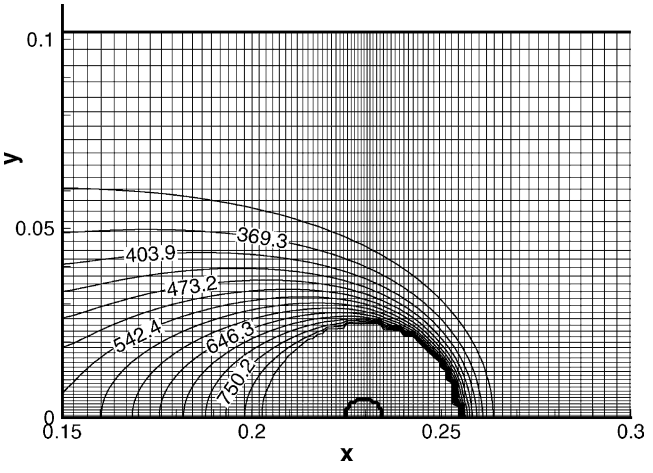

Fig. 8. Detailed results near the tool, t = 30 s, weld period.

the material yield stress, and subsequently make the FSW easier, and is also beneficial to protect the tool from being worn out.

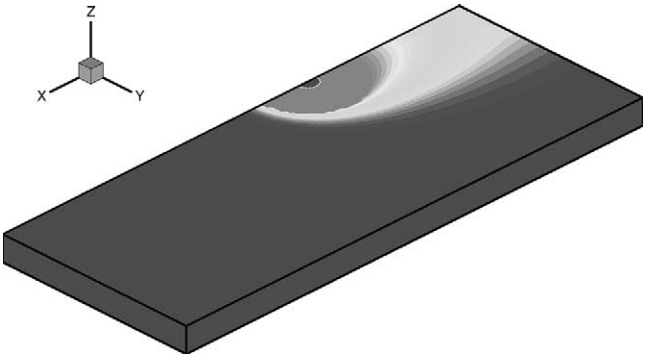

Fig. 9. Calculated isothermals, t= 30 s, welding period, 3-D view.

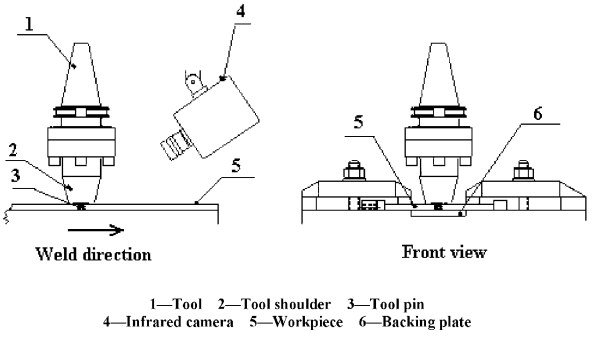

Fig. 10. Diagram of the experimental setup.

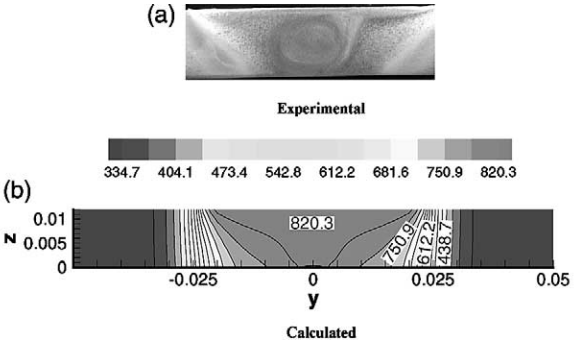

Fig. 11. Comparison between the peak temperature and the microstructure morphology.

5. Conclusion

A three-dimensional transient heat-transfer model in a moving coordinate has been developed in this paper; the calculated results successfully demonstrated the heat-transfer process of the workpiece in friction stir welding. The following conclusions can be drawn:

1. This model can accurately model the heat-transfer process in FSW. The difficulty of determining the temperature distribution near the moving tool pin has been reduced.
2. Because a moving coordinate is introduced, no mov-

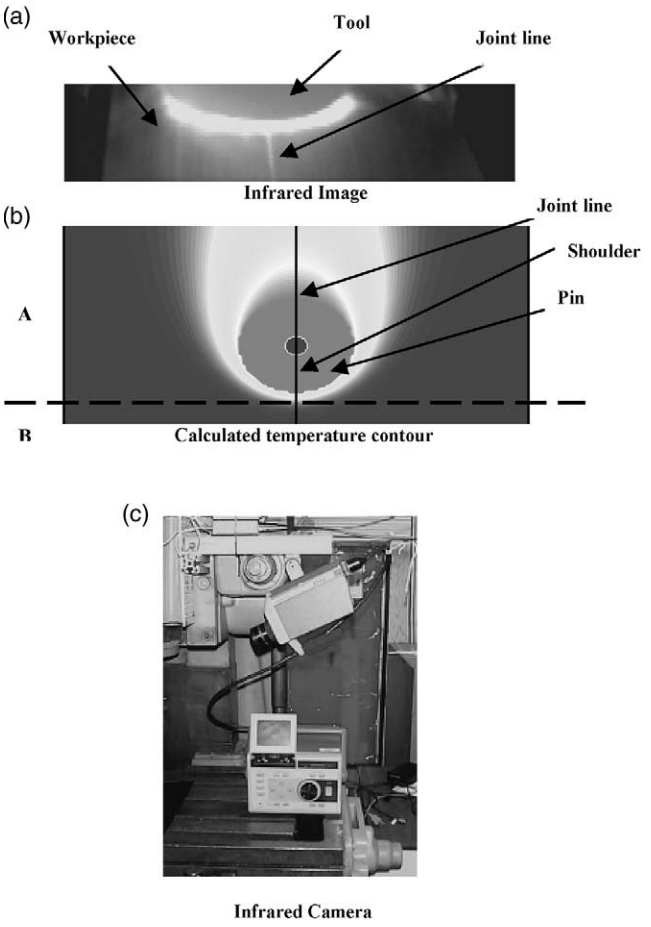

Fig. 12. Comparison between the infrared image and calculated temperature.

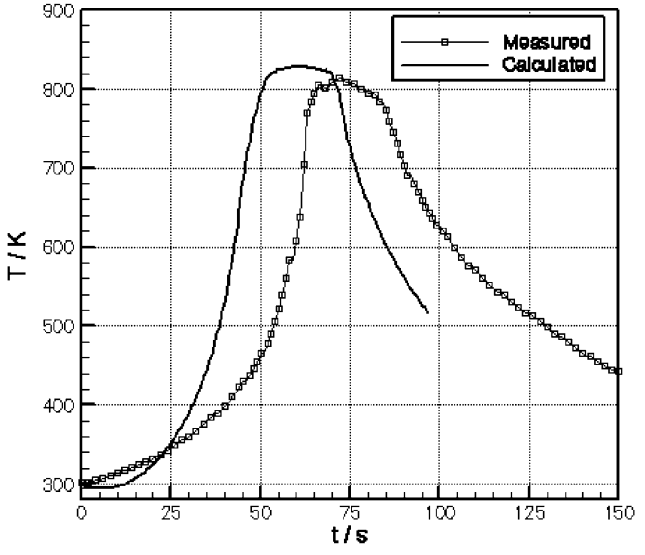

Fig. 13. Calculated and measured temperatures at measuring point 1.

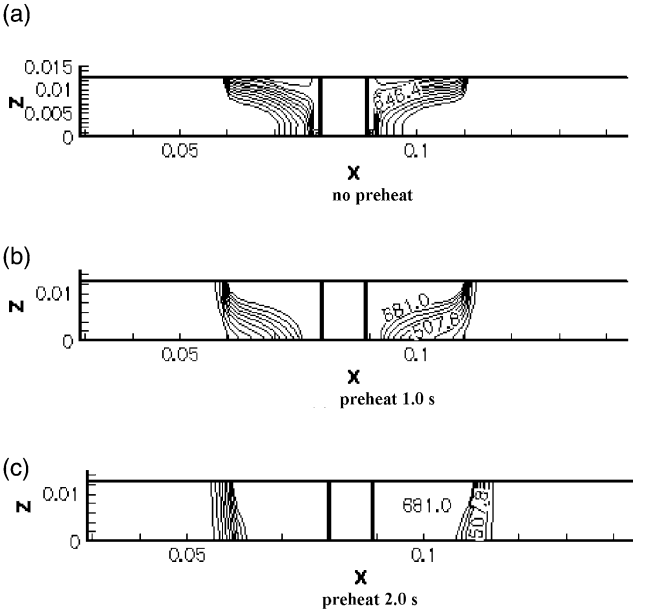

Fig. 14. Calculated temperature contour at different preheat time, side view.

ing heat source needs to be modeled; therefore, this model can be easily applied to model the coupled heat-transfer process for both the tool and the workpiece during FSW.

3. A preheat is beneficial to increase the temperature of the workpiece in front of the tool pin, making the material easy to be welded, while protecting the tool from being worn out.

Acknowledgements

The authors would like to express thanks to Mr. M. Valant, Mrs. D. Jandric and Dr. J. Ouyang from SMU for their valuable help during the experiments and part of this research.

This work is financially supported by the U.S. Department of Education, Grant No. P200A80806-98; and by the Texas High Education Coordinating Board, Grants No.003613-022-1999 and No.003613-0016-2001.

References

[1] M.W. Thomas, J. Nicholas, J.C. Needham, M.G. Murch, P. Templesmith, C.J. Dawes, Friction Stir Butt welding, GB Patent Application No.9125978.8 Dec 1991. US Patent No.5460317, Oct. 1995.

[2] W. Thomas, P. Threadgill, E. Nicholas, The feasibility of friction stir welding steel, Science and Technology of Welding and Joining 4 (6) (1999).

[3] C.J. Dawes, An introduction to friction stir welding butt welding and its developments, Welding and Fabrication Jan (1995).

[4] E.D. Nicholas et al. Friction stir welding—a decade on, IIW

Asian Pacific International Congress, Sydney, Oct.29-Nov.2, 2000.
[5] Y.J. Chao, X. Qi, Thermal and thermo-mechanical modeling of friction stir welding of aluminum alloy - 6061-T6, Journal of Materials Processing & Manufacturing Science 7 (1998).
[6] Ø. Frigaard, Ø. Grong, O.T. Midling, Modeling of the heat flow phenomena in friction stir welding of aluminum alloys, Proceedings of the Seventh International Conference Joints in Aluminum—INALCO '98, Cambridge, UK, April 15-17, 1998.
[7] Ø. Frigaard, Ø. Grong, O.T. Midling, A process model for friction stir welding of age hardening aluminum alloys, Metallurgical and Materials Transactions A 32A (2001).
[8] J.E. Gould, Z. Feng, Heat flow model for friction stir welding of aluminum alloys, Journal of Material Processing and Manufacturing Science 7 (1998).
[9] M.J. Russell, H.R. Shercliff, Analytical modeling of microstructure development in friction stir welding, Proceedings of the first International Symposium on Friction Stir Welding, Thousand Oaks, CA June 1999.
[10] M. Zahedul, H. Khandkar, J. Khan, Thermal modeling of overlap friction stir welding for Al-alloys, Journal of Material Processing and Manufacturing Science 10 (2001).
[11] G.B. Bendzsak, T.H. North, C.B. Smith, An experimentally validated 3D model for friction stir welding, Proceedings of the second International Symposium on Friction Stir Welding, Sweden, August 2000.
[12] C.B. Smith, G.B. Bendzsak, T.H. North, J.F. Hinrichs, J.S. Noruk, R.J. Heideman, Heat and material flow modeling of the friction stir welding process, Proceedings of Ninth International Conference on Computer Technology in Welding, in: T. Siewert, C. Pollock (Eds.), May 2000.
[13] P. Colegrove, Three dimensional flow and thermal modeling of the friction stir welding process, Proceedings of the second International Symposium on Friction Stir Welding, Sweden, August 2000.
[14] G. Kohn, Laser-assisted friction stir welding, Welding Journal Feb (2002) 46–48.
[15] M. Song, R. Kovacevic, A new heat transfer model for friction stir welding, Accepted by Journal of Engineering Manufacturing.
[16] P. Dong, F. Lu, J.K. Hong, Z. Cao, Analysis of weld formation process in friction stir welding, Proceedings of the first International Symposium on Friction Stir Welding, Thousand Oaks, CA June 1999.
[17] A. Askari, S. Silling, B. London, M. Mahoney, Modeling and analysis of friction stir welding process, in: K. Jata, M. Mahoney, R.S. Mishra, S.L. Semiatin, D.P. Field (Eds.), Friction Stir Welding and Processing, TMS, 2001.
[18] R.W. Fonda, S.G. Lambrakos, Analysis of friction stir welding using an inverse-problem approach, in: K. Jata, M. Mahoney, R.S. Mishra, S.L. Semiatin, D.P. Field (Eds.), Friction Stir Welding and Processing, TMS, 2001.
[19] M. Song, R. Kovacevic, A new heat transfer model for friction stir welding, Transaction of NAMRI/SME, Vol. XXX, 2002.
[20] W. Tang, X. Guo, J.C. McClure, L.E. Murr, Heat input and temperature distribution in friction stir welding, Journal of Materials Processing & Manufacturing Science 7 (1998).
[21] M.W. Mahoney, C.G. Rhodes, J.G. Flintoff, R.A. Spurling, W.H. Bingel, Properties of friction-stir-welded 7075 T651 aluminum, Metallurgical and Materials Transactions A 29A (1998).
[22] A.P. Reynolds, et al. Processing-property correlation in friction stir welds, Materials Science Forum 331-337 (2000) 1719–1724.
[23] Y. Sato, H. Kokawa, M. Enomoto, S. Jogan, Microstructure evaluation of 6063 aluminum during friction stir welding, Metallurgical and Materials Transaction A 30 A (1999) 2429–2437.
[24] F. Grong, Metallurgical Modeling of Welding, second ed, The Institute of Materials, 1993.
[25] B. Wands, Thermal stress analysis of side-installed NuMi absorber, MSG-EAR-01285, Fermilab, April 2001.